ISSN: 0067-2904

Evidences of the sturdy domination of short-range effect on Coulomb form factors in the atomic nucleus ^{60}Ni

Altaf A. Al-Rahmani[1*], Adel K. Hamoudi[2]
[1]*Department of Physics, College of Science for Women, University of Baghdad, Baghdad, Iraq*
[2] *Department of Optics Techniques, Al-Farabi University College, Baghdad, Iraq*

Received: 6/5/2024 Accepted: 9/ 7/2025 Published: 30/6/2026

Abstract

Inelastic Coulomb form factors with inclusion of the effect of short-range correlation functions for certain assignment excitations (such as 2^+ (1.33), 2^*(2.16), 4^*(2.50), 4^*(3.13), 4^*(3.67), 3^-(4.04), 3^-(6.20), and 3^-(7.05) MeV) as well as for uncertain assignment excitations (such as 4.85 (2^+, 4^+), 5.05 (4^+, 6^+) and 6.85 (2^+, 5^-) MeV) in ^{60}Ni atomic nucleus have been scrutinized. The form factors of uncertain assignment excitations have been computed by decomposing the excitations 4.85, 5.05 and 6.85 MeV to (C2 and C4), (C4 and C6), and (C2 and C5) components, respectively. The charge density of the ^{60}Ni has been also scrutinized using the one- and two-particle parts of cluster extension in collaboration with single-particle harmonic wave functions. The short-range correlation of Jastrow formula, which relies on the correlation parameter (β), has been incorporated into the two-particle part of cluster extension The nucleus of ^{60}Ni consists of a ^{56}Ni-core plus four energetic neutrons dispersed in f5p-model space, where this nucleus has no energetic protons outer the ^{56}Ni-core. Thus, inelastic Coulomb form factors of ^{60}Ni have been exclusively computed from the core polarization transition charge density using Tassie formulation, relying on the computed charge density. The oscillator parameter (b) and correlation parameter (β) have been applied to existing calculations, where b and β have been independently created for every specific nucleus through matching between the anticipated and measured elastic form factors. In this study, a single value for each of b and β has been used to compute the inelastic form factors for diverse excitations in ^{60}Ni, where the computed results show a well accordance with available data. It is concluded that the influence of short-range correlation functions rules substantially the existing computations, where this effect seems to be crucial to creating an important modification to the predicated findings which ultimately leads to elucidate the data astoundingly across all assumed momentum transfers.

Keywords: Electron scattering; Elastic and inelastic form factors; Nuclear density; Short- range effects; ^{60}Ni atomic nucleus.

أدلة على الهيمنة القوية لتأثير المدى القصير على عوامل التشكل الكولومية في النواة الذرية ^{60}Ni

الطاف عبد المجيد الرحماني[1]*, عادل خلف حمودي[2]
[1]قسم الفيزياء، كلية العلوم للبنات، جامعة بغداد، بغداد، العراق
[2]قسم التقنيات البصرية، كلية الفارابي الجامعة، بغداد، العراق

*Email: altafha_phys@csw.uobaghdad.edu.iq

الخلاصة

تم دراسة عوامل التشكل الكولومية الغير مرنة ، مع تضمين تأثير دوال ارتباط المدى القصير ، لحالات الأثارة المؤكدة (مثل 2^+ (1.33) ، 2^+ (2.16) ، 4^+ (2.50) ، 4^+ (3.13) ، 4^+ (3.67) ، 3^-(4.04) ، 3^-(6.20) و 3^-(7.05) MeV) وكذلك لحالات الأثارة الغير مؤكدة (مثل 4.85 (2^+ ، 4^+) ، 5.05(4^+ ، 6^+) و 6.85 (2^+ ، 5^-) MeV) في النواة الذرية ^{60}Ni. تم حساب عوامل التشكل لحالات الأثارة الغير مؤكدة من خلال تحليل الأثارات 4.85 ، 5.05 و 6.85 MeV الى المركبات (C2 و C4) ، (C4 و C6) و (C2 و C5) ، على التوالي. أيضًا تم دراسة كثافة الشحنة لنواة ^{60}Ni من خلال استخدام حد الجسيم المنفرد وحد الجسيمتين من امتداد كلاستر (Cluster expansion) وبأستخدام الدوال الموجية التوافقية للجسيم المنفرد. تم ادخال دالة ارتباط المدى القصير لصيغة جاسترو (Jastrow formula) ، المعتمدة على معلمة الأرتباط (β) ، في حد الجسيمتين من امتداد كلاستر. تتألف نواة ^{60}Ni من القلب المغلق ^{56}Ni مع أربعة نيوترونات نشطة تتحرك ضمن أنموذج الفضاء f5p ، حيث هذه النواة لا تحتوي على بروتونات نشطة خارج القلب المغلق ^{56}Ni. لذا فأن عوامل التشكل الكولومية الغير مرنة في النواة ^{60}Ni قد تم حسابها حصريا من كثافة الشحنة الأنتقالية لأستقطاب القلب بأستخدام صيغة تاسي (Tassie form)، بالأعتماد على كثافة الشحنة المحسوبة. تم تطبيق معلمة المتذبذب b ومعلمة الأرتباط β في الحسابات الحالية ، حيث يتم توليدهما بشكل مستقل لكل نواة مميزة عن طريق المطابقة بين عوامل التشكل المرنة المتوقعة والفعلية. في الدراسة الحالية تم استخدام قيمة واحدة لكل من b و β في حساب عوامل التشكل الغير المرنة لحالات الأثارة المختلفة في النواة ^{60}Ni ، حيث تظهر النتائج المحسوبة توافقا جيدا مع ما هو متوفر من بيانات عملية. نستنتج من هذه الدراسة بأن تأثير دوال ارتباط المدى القصير يهيمن بشكل كبير على الحسابات الحالية ، حيث يبدو أن هذا التأثير حاسم لإنشاء تعديل مهم للنتائج المتوقعة مما يؤدي في النهاية إلى تفسير جدير بالملاحظة للبيانات عبر جميع عمليات نقل الزخم المفترضة.

1. Introduction

The atomic nucleus is recognized as the supreme convoluted structure. Understanding how the short inter-particle piece of wave function works is fundamental for explaining nuclei. The difficult task is a result of the convoluted interactions amid nucleons and the substantial nuclear density. Besides, it ensures that all important measurements of the nucleus (for example, the mean distance, the interaction range and the nucleon size) to be accurate, which makes real theoretical explications to some extent hard [1]. The structure of the neutron [2, 3], the bound nucleon [4–8], in addition to the investigations of neutrino oscillations and neutrino-nucleus interactions [9–13], all rely notably on having a comprehensive concerned of short-range correlations (SRCs).

Existent models of the average field aptly explicate various static features [14] in nuclei; nonetheless they don't prosper in elucidating how the SRCs dynamic affects these features. Ab-initio predictions of many-particle system [15–18] are still classified for light shell nuclei with soft interactions that modify short-range component of the wave function. Hence, actual models are still favored to sort the principal physical process at short distances and to explicate the middle in addition to the high mass nuclei [19–21].

The consolidation of SRCs into the Slater determinant was fulfilled by studies [22-24], involving commonly $N = Z$ light nuclei from the standpoint of Born approximation These studies tried to establish a formulation for elastic form factors, $F_{el}(q)$, abbreviated at two particle fragments using the factor cluster expansion [25-27]. This formulation was employed to open s-, p-, as well as sd-shell nuclei in addition to closed (^{4}He, ^{16}O and ^{40}Ca) nuclei. The effect of SRCs on the s, p, and sd shell nuclei were attained by [28] with utterly different from the tactic employed by [22–24]. Cluster expansion and Jastrow function, which interpolates SRCs, were used by [29] for creating apparent formulations to elastic form

factors $F_{el}(q)$ and densities $\rho(r)$. In fact, these formulations are reliant on the single particle motion [30,31] as an alternative of the relative two-particle wave functions [21]. It is fundamental to indicate that the studies listed above were uniquely joined with the influence of SRCs on elastic $F_{el}(q)$.

In this research, the effect of SRCs on inelastic form factors $F_{inel}(q)$ of the ^{60}Ni nucleus has been searched for a number of excited states using a single value for each of *b* and β, where the existing calculations have been noticeably controlled by this effect. It is found that the effect of SRCs is a crucial for producing a substantial amendment to the predicated findings which ultimately leads to explain the data through all supposed momentum transfers.

2. Theory

Inelastic form factor for scattering of electron from nucleus is expressed as [32]:

$$\left|F_J^L(q)\right|^2 = \frac{4\pi}{Z^2(2J_i+1)}\left|\left\langle f \left\| \hat{T}_J^L(q) \right\| i \right\rangle\right|^2 \left|F_{cm}(q)\right|^2 \left|F_{fs}(q)\right|^2, \tag{1}$$

where q and J symbolize the momentum transfer and angular momentum, $|i\rangle = |J_i T_i\rangle$ and $|f\rangle = |J_f T_f\rangle$ symbolize the initial and final states considered as $J_{i/f}$ (spin) and $T_{i/f}$ (isospin), $\hat{T}_J^L(q)$ symbolizes the electron-nucleus scattering, $F_{cm}(q) = e^{q^2b^2/4A}$ symbolizes the center of mass (cm) correction (which is accountable for ignoring untruthful states created from the center of mass motion after using the wave function of the shell model), $F_{fs}(q) = e^{-0.43q^2/4}$ symbolizes the finite-sized nucleon (fs) correction (which is rumored to be alike for neutron as well as proton), Z and A symbolize the atomic and mass numbers, correspondingly, and $b = \sqrt{\hbar/(M_p\omega)}$ [33] symbolizes the oscillator size parameter, where h symbolizes Plank's constant and $\hbar = h/2\pi$, M_p symbolizes the mass of proton and ω symbolizes the angular frequency. Reducing the matrix presented in Eq. (1) gives [34]:

$$\begin{aligned}\left|F_J^L(q)\right|^2 = \frac{4\pi}{Z^2(2J_i+1)}&\left|\sum_{T=0,1}(-1)^{T_f-T_{Z_f}}\begin{pmatrix} T_f & T & T_i \\ -T_{z_f} & 0 & T_{z_i}\end{pmatrix}\left\langle J_f T_f \left\|\hat{T}_{JT}^L(q)\right\| J_i T_i \right\rangle\right|^2 \\ &\times \left|F_{cm}(q)\right|^2 \left|F_{fs}(q)\right|^2.\end{aligned} \tag{2}$$

The bracket, in Eq.2, signifies the 3*j*- symbol, while *T* (isospin) and T_z (isospin projection) are demarcated by

$$\left|T_f - T_i\right| \le T \le T_f + T_i \text{ while } T_Z = \frac{Z-N}{2}. \tag{3}$$

The abridged matrix, displayed in Eq. (2), is delineated by [33]:

$$\left\langle f \left\| \hat{T}_{JT}^L \right\| i \right\rangle = \sum_{a,b} OBDM^{JT}(i,f,J,a,b)\left\langle b \left\| \hat{T}_{JT}^L \right\| a \right\rangle. \tag{4}$$

Here the states of single-particle are demarcated by *a* as well as *b*. The One-Body Density Matrix (OBDM), revealed in Eq. (4), is assessed by [35]:

$$OBDM(\tau_z) = (-1)^{T_f - T_Z} \begin{pmatrix} T_f & 0 & T_i \\ -T_z & 0 & T_z \end{pmatrix} \sqrt{2}\, \frac{OBDM(\Delta T = 0)}{2} + \tau_z (-1)^{T_f - T_Z} \begin{pmatrix} T_f & 1 & T_i \\ -T_z & 0 & T_z \end{pmatrix} \sqrt{6}\, \frac{OBDM(\Delta T = 1)}{2}, \tag{5}$$

here τ_z defines the isospin operator of single particle.

To engender the many-body reduced matrix elements of the $\hat{T}_J^L(q)$ operator, the model space (ms) as well as core polarization (cp) involvements are added [35]:

$$\left\langle f \left\| \hat{T}_J^L(\tau_Z, q) \right\| i \right\rangle = \left\langle f \left\| \hat{T}_J^{ms L}(\tau_Z, q) \right\| i \right\rangle + \left\langle f \left\| \hat{T}_J^{cp L}(\tau_Z, q) \right\| i \right\rangle. \tag{6}$$

The involvement of the ms, displayed in Eq. (6), is defined by:

$$\left\langle f \left\| \hat{T}_J^{ms L}(\tau_Z, q) \right\| i \right\rangle = \int_0^\infty d\mathrm{r}\, \mathrm{r}^2\, j_J(q\mathrm{r})\, \rho_{J,\tau_Z}^{ms}(i, f, \mathrm{r}), \tag{7}$$

where $j_J(qr)$ designates the spherical Bessel function, and $\rho_{J,\tau_Z}^{ms}(i, f, r)$ designates the ms transition charge density defined by [35]:

$$\rho_{J,\tau_Z}^{ms}(i, f, \mathrm{r}) = \sum_{jj'(ms)}^{ms} OBDM(i, f, J, j, j', \tau_z)\, \left\langle j \left\| \mathrm{Y}_J \right\| j' \right\rangle R_{nl}(\mathrm{r})\, R_{n'l'}(\mathrm{r}), \tag{8}$$

where $R_{nl}(r)$ and Y_J designate the radial and spherical parts of the wave function, respectively.

The involvement of the cp, in Eq. (6), is defined by:

$$\left\langle f \left\| \hat{T}_J^{cp L}(\tau_Z, q) \right\| i \right\rangle = \int_0^\infty d\mathrm{r}\, \mathrm{r}^2\, j_J(q\mathrm{r})\, \rho_{J,\tau_Z}^{cp}(i, f, \mathrm{r}), \tag{9}$$

where $\rho_{J\tau_Z}^{cp}(i, f, r)$ designates the cp transition charge density, that defines the nuclear collective modes and depends on the formulation utilized for cp. So the complete transition charge density has the form:

$$\rho_{J\tau_Z}(i, f, r) = \rho_{J\tau_Z}^{ms}(i, f, r) + \rho_{J\tau_Z}^{cp}(i, f, r) \tag{10}$$

In this investigation, $\rho_{J\tau_Z}^{cp}(i, f, r)$ is rumored to hold the formulation of Tassie [36]:

$$\rho_{Jt_Z}^{cp}(i, f, r) = N_T\, \frac{1}{2}(1 + \tau_z)\, r^{J-1}\, \frac{d\rho_{ch}^{gs}(i, f, r)}{dr}, \tag{11}$$

where

$$N_T = \frac{\int_0^\infty dr\, r^{J+2} \rho_{t_Z}^{ms}(i, f, r) - \sqrt{(2J_i + 1)\, B(CJ)}}{(2J+1)\int_0^\infty dr\, r^{2J} \rho_{ch}^{gs}(i, f, r)}, \tag{12}$$

defines the normalization constant created by amending of the reduced transition intensity $B(CJ)$ to the observed one, and $\rho_{ch}^{gs}(i, f, r)$ defines the nuclear charge density of ground state.

Note that the density $\rho_{ch}^{gs}(r)$ of closed shell nuclei (with $N = Z$) may be allied to that of point nucleon density $\rho_p^{gs}(r)$ by:

$$\rho_{ch}^{gs}(r)=\frac{1}{2}\rho_{p}^{gs}(r). \tag{13}$$

To accommodate the SRCs effects into $\rho_{p}^{gs}(r)$, the wave function of many-particle is given by:

$$\Psi = F\,\Phi, \tag{14}$$

where F indicates a model operator that inserts Short Range Correlations (SRCs) and Φ denotes the wave function of Slater determinant. In this investigation, F is chosen as a Jastrow model [29]:

$$F=\prod_{i<j}^{A} f(r_{ij}), \tag{15}$$

where $f(r_{ij})=f(\left|\vec{r}_i-\vec{r}_j\right|)$, which defines the two-body SRCs, is a state autonomous function defined by:

$$f(r_{ij})=1-\exp[-\beta(\vec{r}_i-\vec{r}_j)^2], \tag{16}$$

which holds the properties: $f(r_{ij})\to 1$ when $\vec{r}_{ij}=\left|\vec{r}_i-\vec{r}_j\right|$ is big and $f(r_{ij})\to 0$ when $\vec{r}_{ij}\to 0$. Thus, the effectt of SRCs, implanted by Eq. (16), becomes larger for small values of SRC parameter β and vice versa.

An obvious formulation to $\rho_{p}^{gs}(r)$ is written as [28]:

$$\begin{aligned}\rho_{p}^{gs}(r) &= N_D\left\langle\Psi(\vec{r}_1,\vec{r}_2,...,\vec{r}_A)\right|\hat{O}_r\left|\Psi(\vec{r}_1,\vec{r}_2,...,\vec{r}_A)\right\rangle\\ &= N_D\left\langle\hat{O}_r\right\rangle,\end{aligned} \tag{17}$$

where $\Psi(\vec{r}_1,\vec{r}_2,...,\vec{r}_A)$ is the nuclear wave function of many-particle system displayed in Eq. (14), $N_D=\left\langle\Psi(\vec{r}_1,\vec{r}_2,...,\vec{r}_A)\right|\Psi(\vec{r}_1,\vec{r}_2,...,\vec{r}_A)\rangle^{-1}$ is a constant created by: $4\pi\int_0^{\infty}\rho_{p}^{gs}(r)r^2dr=1$, while $\hat{O}_r$ defines the one-body density operator given by:

$$\hat{O}_r=\sum_{i=1}^{A}\hat{o}_r(i)=\sum_{i=1}^{A}\delta(\vec{r}-\vec{r}_i). \tag{18}$$

To determine $\rho_{p}^{gs}(r)$, the integral of generalized normalization was employed [28]:

$$I(\alpha)=\left\langle\Psi\right|[\exp[\alpha\, I(0)\,\hat{O}_r\left|\Psi\right\rangle, \tag{19}$$

like the operator $\hat{O}_r$ from:

$$\left\langle\hat{O}_r\right\rangle=\left[\frac{\partial\ln I(\alpha)}{\partial\alpha}\right]_{\alpha=0}. \tag{20}$$

In cluster inquest of Eq. (20), the integrals $I_i(\alpha)$, $I_{ij}(\alpha)$ . . . were employed for segments of a system that has A-particles and a factor cluster disassembly of these integrals. Then $\rho_{p}^{gs}(r)$ is formulated as [28]:

$$\rho_{p}^{gs}(r)=N_D\left\langle\hat{O}_r\right\rangle=N_D\left\{\left\langle\hat{O}_r\right\rangle_1+\left\langle\hat{O}_r\right\rangle_2+...+\left\langle\hat{O}_r\right\rangle_A\right\}, \tag{21}$$

where:

$$\left\langle\hat{O}_r\right\rangle_1=\sum_{i=1}^{A}\left[\frac{\partial\ln I_i(\alpha)}{\partial\alpha}\right]_{\alpha=0}=\sum_{i=1}^{A}\left\langle i\right|F_1^{+}\hat{o}_r(1)F_1\left|i\right\rangle, \tag{22}$$

$$\begin{aligned}\left\langle \hat{O}_r \right\rangle_2 &= \sum_{i<j}^{A} \frac{\partial}{\partial \alpha} \left[\ln I_{ij}(\alpha) - \ln I_i(\alpha) - \ln I_j(\alpha) \right]_{\alpha=0} \\ &= \sum_{i<j}^{A} \left\langle ij \left| F_{12}^{+} [\hat{o}_r(1) + \hat{o}_r(2)] F_{12} \right| ij \right\rangle_a - \sum_{i<j}^{A} \left[\left\langle i|\hat{o}_r(1)|i \right\rangle + \left\langle j|\hat{o}_r(2)|j \right\rangle \right],\end{aligned} \tag{23}$$

and so on. Here, the identity is denoted by F_1.

The cluster extension aims to breaking up of one-particle, two-particle, …, A-particle correlation effects on the density. Here, three-particle as well as higer-particle components would not be employed. As a result, the correlated density $\rho_p^{gs}(r)$ of Eq. (21) amends into:

$$\rho_p^{gs}(r) \approx N_D \left\{ \left\langle \hat{O}_r \right\rangle_1 + \left\langle \hat{O}_r \right\rangle_2 \right\}. \tag{24}$$

Using Eqs. (22) and (23) into Eq. (24), we find:

$$\rho_p^{gs}(r) \approx N_D \left\{ \sum_{i=1}^{A} \left\langle i|\hat{o}_r(1)|i \right\rangle + 2\sum_{i<j}^{A} \left\langle ij \left| F_{12}^{+} \hat{o}_r(1) F_{12} \right| ij \right\rangle_a - 2\sum_{i<j}^{A} \left\langle ij|\hat{o}_r(1)|ij \right\rangle_a \right\}. \tag{25}$$

For simplicity, Eq. (25) can be specified as:

$$\rho_p^{gs}(r) \approx N_D \left\{ \left\langle \hat{O}_r \right\rangle_1 + \left\langle \hat{O}_r \right\rangle_{22} - \left\langle \hat{O}_r \right\rangle_{21} \right\} \tag{26}$$

where

$$\left\langle \hat{O}_r \right\rangle_1 = \sum_{i=1}^{A} \left\langle i|\hat{o}_r(1)|i \right\rangle, \tag{27}$$

$$\left\langle \hat{O}_r \right\rangle_{22} = 2\sum_{i<j}^{A} \left\langle ij \left| F_{12}^{+} \hat{o}_r(1) F_{12} \right| ij \right\rangle_a, \tag{28}$$

$$\left\langle \hat{O}_r \right\rangle_{21} = 2\sum_{i<j}^{A} \left\langle ij|\hat{o}_r(1)|ij \right\rangle_a. \tag{29}$$

Using the form of the two-body SRCs of Eq. (16), then:

$$\begin{aligned}F_{12}F_{12} &= \left(1 - \exp[-\beta(\vec{r}_1 - \vec{r}_2)^2]\right)\left(1 - \exp[-\beta(\vec{r}_1 - \vec{r}_2)^2]\right) \\ &= 1 - 2g(r_1, r_2, \beta) + g(r_1, r_2, 2\beta)\end{aligned} \tag{30}$$

where:

$$g(r_1, r_2, z) = \exp(-z\, r_1^2) \exp(-z\, r_2^2) \exp(2\, z\, r_1\, r_2 \cos w_{12}), \qquad (with\ z = \beta\ or\ 2\beta). \tag{31}$$

With the assistance of Eqs. (30) and (31), Eq. (28) changes to:

$$\begin{aligned}\left\langle \hat{O}_r \right\rangle_{22} &= 2\sum_{i<j}^{A} \left\langle ij|\hat{o}_r(1) \left[1 - 2g(r_1, r_2, \beta) + g(r_1, r_2, 2\beta) \right] |ij \right\rangle_a \\ &= 2\left\{ \sum_{i<j}^{A} \left\langle ij|\hat{o}_r(1)|ij \right\rangle_a - 2\sum_{i<j}^{A} \left\langle ij|\hat{o}_r(1)\, g(r_1, r_2, \beta)|ij \right\rangle_a + \sum_{i<j}^{A} \left\langle ij|\hat{o}_r(1)\, g(r_1, r_2, 2\beta)|ij \right\rangle_a \right\}\end{aligned} \tag{32}$$

For simplicity, Eq. (32) is set as:

$$\left\langle \hat{O}_r \right\rangle_{22} = \left\langle \hat{O}_r \right\rangle_{21} - 2O_{22}(r, \beta) + O_{22}(r, 2\beta), \tag{33}$$

where

$$O_{22}(r,z)=2\sum_{i<j}^{A}\left\langle ij\left|\hat{o}_r(1)\,g(r_1,r_2,z)\right|ij\right\rangle_a . \tag{34}$$

Using Eq. (33) into Eq. (26), we find:

$$\rho_p^{gs}(r)\approx N_D\left\{\left\langle\hat{O}_r\right\rangle_1-2O_{22}(r,\beta)+O_{22}(r,2\beta)\right\}, \tag{35}$$

where $\rho_p^{gs}(r)$ is in requisite of β implanted by Eq. (16).

The one-body part $\left\langle\hat{O}_r\right\rangle_1$, revealed in Eq. (35), is clearly recognized by:

$$\begin{aligned}\left\langle\hat{O}_r\right\rangle_1&=\sum_{i=1}^{A}\left\langle i\left|\hat{o}_r(1)\right|i\right\rangle\\&=4\sum_{nl}\eta_{nl}(2l+1)\frac{1}{4\pi}\phi_{nl}^{*}(r)\,\phi_{nl}(r),\end{aligned} \tag{36}$$

where $\phi_{nl}(r)$ and η_{nl} represent the radial component of single-particle wave function and the occupation probability of the state nl, respectively. With algebra of spherical harmonics, the formulation of $O_{22}(r,z)$ exhibited in Eq. (34) amends to [28]:

$$\begin{aligned}O_{22}(r,z)=4&\sum_{n_il_i,n_jl_j}\eta_{n_il_i}\eta_{n_jl_j}(2l_i+1)(2l_j+1)\\&\times\left\{4A_{n_il_in_jl_j}^{n_jl_jn_il_i0}(r,z)-\sum_{k=0}^{l_i+l_j}\left\langle l_i0l_j0\left|k0\right\rangle\right.^2A_{n_il_in_jl_j}^{n_jl_jn_il_ik}(r,z)\right\},\qquad(z=\beta,\,2\beta)\end{aligned} \tag{37}$$

where

$$\begin{aligned}A_{n_1l_1n_2l_2}^{n_3l_3n_4l_4k}(r,z)=&\frac{1}{4\pi}\phi_{n_1l_1}^{*}(r)\phi_{n_3l_3}(r)\exp(-zr^2)\\&\times\int_0^{\infty}\phi_{n_2l_2}^{*}(r_2)\phi_{n_4l_4}(r_2)\exp(-zr_2^2)\;i_k(2zrr_2)r_2^2dr_2\,,\end{aligned} \tag{38}$$

with $\left\langle l_i0l_j0\left|k0\right\rangle\right.$ and $i_k(x)$ represent the Clebsch Gordan coefficient and the modified spherical Bessel function, respectively.

In actual fact, Eqs. (13) - (38) are recommended to the closed shell ($Z = N$) nuclei with η_{nl} = zero or one. For open shell ($Z \neq N$) nuclei, a similar formulations can also be employed but with zero $\le \eta_{nl} \le$ one.

The mean square charge radii is demarcated by:

$$\left\langle r^2\right\rangle=\frac{4\pi}{Z}\int_0^{\infty}\rho_{ch}^{gs}(r)\,r^4dr, \tag{39}$$

where

$$Z=4\pi\int_0^{\infty}\rho_{ch}^{gs}(r)\,r^2dr, \tag{40}$$

is the normalization constant of $\rho_{ch}^{gs}(r)$.

where $F_{el}(q)$ is basically the Fourier transform of $\rho_{ch}^{gs}(r)$. i.e.:

$$F_{el}(q)=\frac{4\pi}{Z}\int_0^{\infty}\rho_{ch}^{gs}(r)j_0(qr)r^2dr \tag{41}$$

Allowing for the corrections of $F_{cm}(q)$ and $F_{fs}(q)$ in Eq. (41), we get:

$$F_{el}(q)=\frac{4\pi}{Z}\int_0^{\infty}\rho_{ch}^{gs}(r)j_0(qr)r^2dr\,F_{cm}(q)F_{fs}(q) \tag{42}$$

3. Results and discussion

The estimations of charge density $(\rho_{ch}^{gs}(r))$, elastic form factors $(F_{el.}(q))$ and inelastic form factors $(F_{inel.}(q))$ in ^{60}Ni nucleus have been executed. Two arrangements of estimations have been made using single-particle harmonic wave functions without (arrangement-1) and with (arrangement-2) SRCs effects. The estimations of arrangement-1 rely only on the parameter b whereas those of arrangement-2 rely on b and β. The amounts of b and β in arrangement-1 (arrangement-2), seen in Table 1, have been produced by revising b (b and β) in a stab to suit the estimated rms radius $<r_{ch}^2>_{cal..}^{1/2}$ (the estimated $<r_{ch}^2>_{cal..}^{1/2}$ and $F_{el}(q)$) with those of experimental outcomes. Table 1 also includes the values of $<r_{ch}^2>_{cal.}^{1/2}$, $<r_{ch}^2>_{\exp}^{1/2}$, and the participation of SRCs, $<r^2>_2^{1/2}=\sqrt{<r_{ch}^2>_{cal.}-<r_{ch}^2>_1}$, for the ^{60}Ni nucleus. As a matter of fact, Table 1 exemplifies that b owns an inequity affiliation: $b(\text{arrangement-1})>b(\text{arrangement-2})$, where inclusion of SRCs enlarges the relative distance amid the nucleons and thus causes to expand the size of the nucleus. Accordingly, it is indispensible to diminish the amount of b that correlates with the nuclear size, which is experimentally firm.

Table 1: The amounts of b, β and the participation of the one- and two-body part to the rms radius $<r_{ch}^2>_{Cal..}^{1/2}$ of ^{60}Ni nucleus. Arrangement-1 stands for the estimations of one-particle part (without considering the effect of SRCs) while arrangement-2 stands for the estimations of one- plus two-particle parts (with considering the effect of SRCs).

Arrangement	b (fm)	β (fm^{-2})	Estimated rms charge radius $[<r_{ch}^2>_{Cal..}^{1/2}]$ (fm)			Experimental rms charge radius $<r_{ch}^2>_{\exp.}^{1/2}$ (fm)
			Without SRCs (one-particle part)	With SRCs (two-particle part)	Total	
1	2.06	0	3. 8135	0	3. 8 135	3.796 ± 0.010 [37]
2	1.897	2.027	3.5125	1.2584	3.7311	

In Fig. 1, the quantities of $F_{el}(q)$ in ^{60}Ni estimated without SRCs (itemized by the dashed line) and with SRCs (itemized by the solid line) are publicized and contrasted with the experimental results (itemized by open circles) [37]. It is manifest that the dashed line predicts wonderfully the open circles at the section of $0\le q\le 1$ fm^{-1} and under predicts them at $q>1$ fm^{-1}. Conversely, incorporating of SRC effects (see the solid line) causes to raise the amount of estimated $F_{el}(q)$ at the second and third loops which consecutively lead to place the estimated outcomes into the location of agreement with the open circles. It is clear that the solid line mimics accurately the first and second minima plus the first, second and third maxima that ascended in the experimental data. Besides, the manner and magnitude of the form factors represented by the solid line are in superb accordance with open circles.

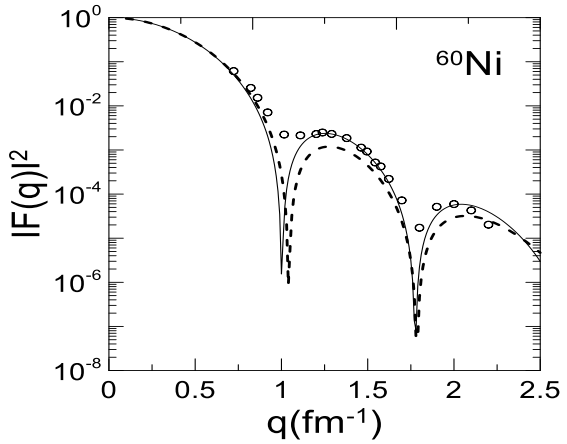

Figure 1: Square of elastic $F(q)$ are displayed as a function of q (fm^{-1}) for the ^{60}Ni nucleus.

The dashed and solid lines stand for the estimated results without and with comprising of SRCs effects, in that order. The open circles stand for the experimental outcomes taken from [37].

In Fig. 2, the density $\rho_{ch}^{gs}(r)$ for the ^{60}Ni estimated without and with the implementation of SRC effects (itemized by the dashed and solid lines, respectively) are displayed and compared with the data (itemized by open circles) [37]. Moreover, the contribution of SRCs $\rho_2(r) = \rho_{ch}^{gs}(r) - \rho_{1,ch}^{gs}(r)$ (itemized by the long dashed line) is also exposed in this figure.

The performance of $\rho_2(r)$ is publicized as fluctuating around the r-axis. This figure illustrates that the likelihood of existing a proton adjacent to the central piece ($0 \le r \le 3$ fm) of $\rho_{ch}^{gs}(r)$ is higher than that of the tail piece ($r > 3$ fm^{-1}). Additionally, the placement of SRCs into $\rho_{ch}^{gs}(r)$ results in a significant decrease in the central piece and a little increase in the tail piece of $\rho_{ch}^{gs}(r)$. This explicates why the adding of SRCs results in an intensification of the possibility of transferring the proton from the central portion of the nucleus to the direction of its surface which in turn causes to amplification of the rms charge radius of the studied nucleus and makes it less rigid than it would be in the absence of SRCs effects. To maintain the nuclear size surrounded by the normal experiential value, the magnitude of b should be lowered when considering for SRCs, see Table 1. Besides, combining the SRCs into $\rho_{ch}^{gs}(r)$ results in developing the outcomes and makes them in better accord with those of observed data.

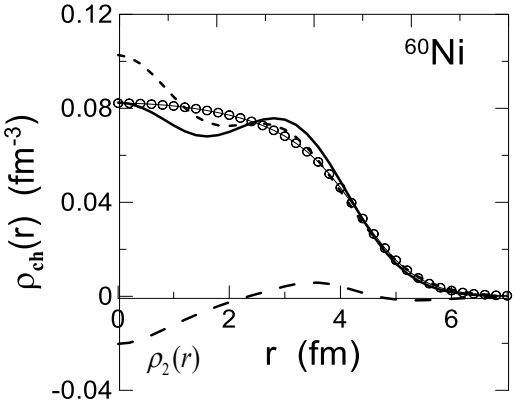

Figure 2: The distribution $\rho_{ch}(r)$ in ^{60}Ni nucleus is plotted against r. The dashed and solid lines are the estimated outcomes without and with involving the short range effects, in that

order. The participating of SRCs effect $\rho_2(r)$ is also displayed in this figure by the long-dashed curve. The experimental data (open circles) is taken from [37].

The effect of SRCs on inelastic form factors $F_{inel}(q)$ of a number of states in ^{60}Ni nucleus is discussed. This nucleus, which owns a total isospin of T= 2, comprises of a ^{56}Ni core and 4 active neutrons distributed in the f5p- space, designated by $2p_{3/2}$, $1f_{5/2}$, and $2p_{1/2}$ orbitals. Due to the absence of active protons outside of the ^{56}Ni-core in the ^{60}Ni, the inelastic form factors entirely come from $\rho^{cp}_{J\tau_Z}(i,f,r)$. The Tassie model, in conjunction with the computed $\rho^{gs}_{ch}(r)$, has been used to determine the cp effects on $F_{inel}(q)$. In this study, the form factors for diverse states in the ^{60}Ni nucleus have been estimated using a single value for each of b and β. These magnitudes of b and β (presented in Table 1) were produced by a fitting to the observed $F_{el}(q)$.

The comparison among the estimated and measured $F_{inel}(q)$ for transitions from the ground (initial) state (J^{π}_i) to unlike final states (J^{π}_f) are shown in Figs. 3-9, where the parities of these transitions in Figs. 3-4, 6-8, and the left panel of Fig. 9 (Fig. 3 and the middle panel of Fig. 9) are similar {dissimilar} between the initial and final states. It is crucial to indicate that all pondered transitions are of isovector-type with $T = 2$ for the ^{60}Ni nucleus. The open circle symbols are the measured outcomes whereas the dashed and solid lines are the arrangement-1 and arrangement-2 estimations achieved without and with the supplement of SRCs, congruently.

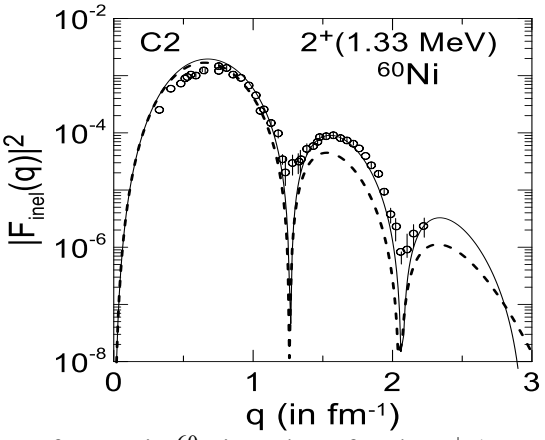

Figure 3: Square of C2 form factors in ^{60}Ni nucleus for the 2^+ (1.33 MeV) state. The dashed and solid lines embody the estimated results produced without and with the attachment of SRCs, in that order. The measured results (open circles) are taken from [38].

In Fig. 3, the estimated and measured outcomes of inelastic C2 form factors $F_{inel.}(q)$ for the transition to the state 2^+_f (with measured excitation energy E_x = 1.33 MeV and reduced transition probability B(C2) = $(7.66\pm0.77)\times10^2$ e^2.fm^4 [38]) are displayed. This figure demonstrates that the C2 outcomes estimated without the SRCs (the dashed line) estimates the data (open circles) tremendously well over the first loop ($q < 1.27$ fm^{-1}) but undervalues considerably the data over the second and third loops ($q \geq 1.27$ fm^{-1}). Embedding the influence of SRCs leads to enhance the result of C2 form factors (the solid lines) at the region of high momentum transfer $q > 1.27$ fm^{-1}, where the data along the first, second and third loops plus along the first and second loops are produced at the correct places by the solid line.

Also, the solid line accurately reproduces the values and presentation of measured C2 results through all maxima and minima. The contrast between the dashed and solid lines shows that the effect of SRCs over the third (second) loop is larger than the second (first) loop.

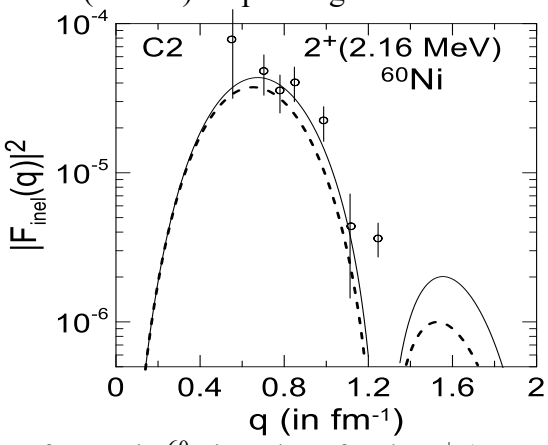

Figure 4: Square of C2 form factors in ^{60}Ni nucleus for the 2^+ (2.16 MeV) state. The dashed and solid lines embody the estimated results produced without and with the attachment of SRCs, in that order. The measured results (open circles) are taken from [38].

In Fig. 4, the calculations of C2 form factors are repeated just as in Fig. 3 but this time for the state 2_f^+ ($E_x = 2.16$ MeV and B(C2) = $(1.5 \pm 0.4) \times 10^1$ e^2.fm^4 [38]). It is clear that the C2 outcomes attained without SRCs (the dashed line) don't forecast accurately the data (open circles) along the considered region of $q \leq 1.2$ fm^{-1}, where these data are underestimated to some extent by this line. Taking into consideration the influence of SRCs causes in improving the C2 outcomes along all considered q. Also, both the performance and values of form factors demonstrated via the solid line show good agreement with the observed data along the first diffraction maximum. Again, the comparison between the dashed and solid lines (which offers the same argument as that found in Fig. 3) demonstrates that the influence of SRCs through the second loop is bigger than the first loop.

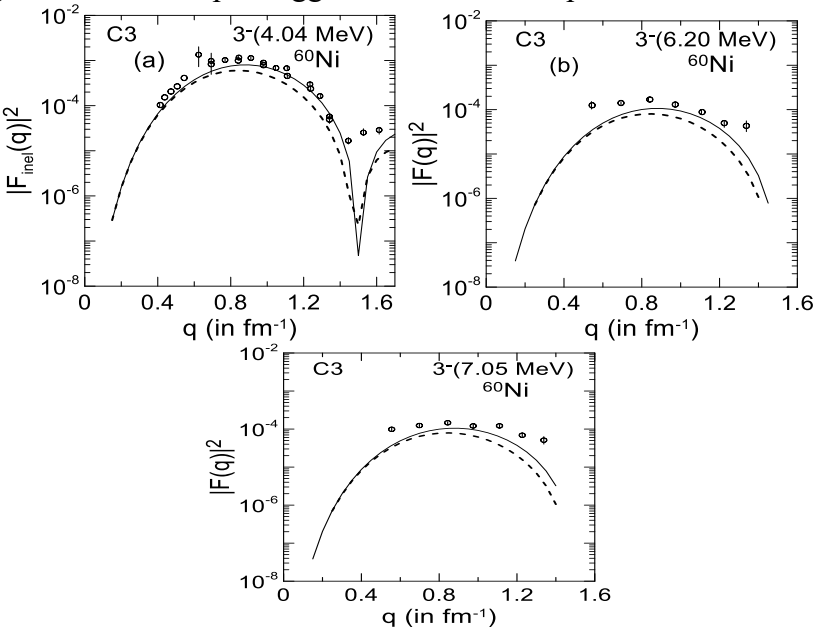

Figure 5: Square of C3 form factors in ^{60}Ni nucleus for 3^- [(a) E_x= 4.04 MeV, (b) E_x= 6.20 MeV) and (c) E_x= 7.05 MeV] states. The dashed and solid lines embody the estimated results produced without and with the attachment of SRCs, in that order. The measured results (open circles) are taken from [38].

In Fig. 5, the C3 results for 3_f^- states [(a): (E_x = 4.04 MeV, B(C3) = $(1.65 \pm 0.25) \times 10^4$ $e^2.fm^6$), (b): (E_x = 6.20 MeV, B(C3) = $(2.20 \pm 0.33) \times 10^3$ $e^2.fm^6$), and (c): (E_x = 7.05 MeV, B(C3) = $(2.17 \pm 0.33) \times 10^3$ $e^2.fm^6$)] [38] are demonstrated. Figs. 3(a-c) show that the C3 findings of the dashed line calculated without SRCs are insufficient for describing the data of open circles [38], where these data are evidently under predicted by these findings. Inserting of the SRCs leads to enhance clearly the C3 findings of the solid line, where generally the estimated results in Fig. 3(a) (Figs. 3(b) and 3(c)) are now in very well (reasonable) accord with the data. Also the performance of the data is well recreated by the solid line.

In Fig. 6, the C4 form factors for 4_f^+ states [(a): (E_x = 2.50 MeV, B(C2) = $(1.5 \pm 0.30) \times 10^5$ $e^2.fm^8$), (b): (E_x = 3.13 MeV, B(C2) = $(3.09 \pm 0.62) \times 10^4$ $e^2.fm^8$), and (c): (E_x = 3.67 MeV, B(C2) = $(5.67 \pm 1.13) \times 10^4$ $e^2.fm^8$)] [38] are shown and compared with those of measured data.

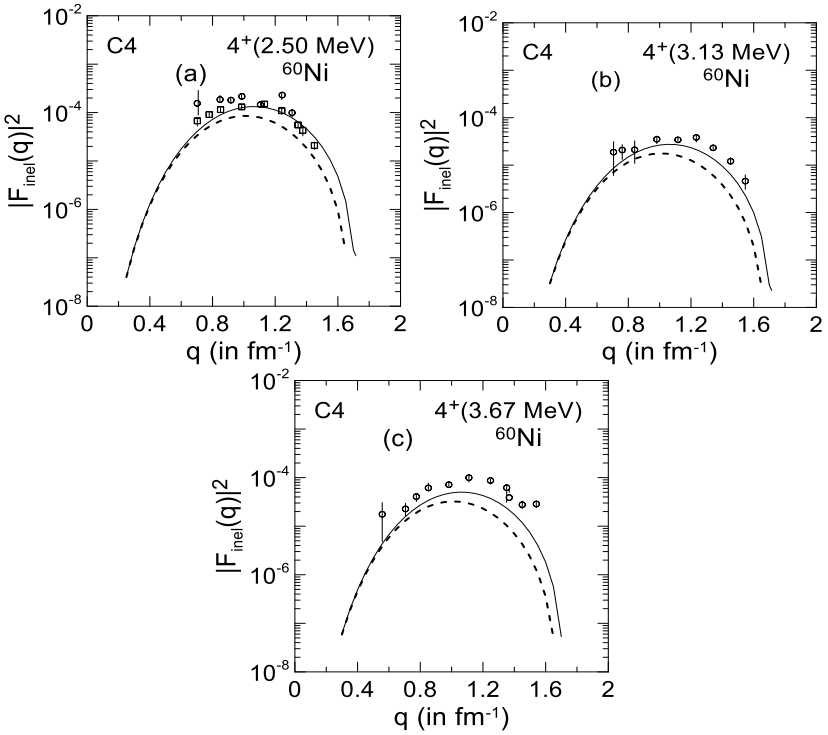

Figure 6: Square of C4 form factors in ^{60}Ni nucleus for 4^+ [(a) E_x= 2.50, (b) E_x= 3.13 and (c) E_x= 3.67 MeV] states. The dashed and solid lines embody the estimated results produced without and with the attachment of SRCs, in that order. The measured results (open circles) are taken from [38].

It is patent that the C4 outcomes without including the influence of SRCs (the dashed lines) are unsatisfactory for explanation the data of open circles [38], where the data are evidently under predicted by these outcomes. Introducing of the SRCs leads to augment the C4 outcomes (the solid lines) through all q values considered in this study, where in general the computed outcomes are now in good accordance with the data. It is obvious that both the manner and magnitudes of the data are well reconstructed by solid lines.

In Fig. 7, the form factors are schemed as opposed to *q* and compared with those of measured outcomes. Here, the measured form factors of E_x = 4.85 MeV are decomposed to

C2 and C4 results using Eqs. (9) and (11) together with the theoretical charge density $\rho_{ch}^{gs}(r)$, obtained through Eqs. (13)-(38). The left panel of this figure shows the C2 results for the state 2^+ (E_x = 4.85 MeV and B(C2) = $(5\pm1)\times10$ $e^2.fm^4$ [38]). The dashed and solid lines signify the C2 form factors calculated without and with supplement of the effect of SRCs whereas those of open circles signify the measured data [38]. It is perceptible that the SRCs don't (do) affect the calculated C2 results over the first (second) loop, where the dashed and solid lines are in coincidence (divergence) with each other. The data at momentum transfer region $0.5 \le q \le 0.85$ ($q > 0.85$) fm^{-1} are in reasonable (poor) agreement with both calculations of the dashed and solid lines. It is apparent from the left panel that the calculated C2 results under forecast evidently the data especially at $q > 0.85$. Thus, the C2 results are not enough to explain the data at all regions of momentum transfer under consideration. In the middle panel, the calculations are recurrent just as in the left panel but this time for C4 results of the state 4^+ (E_x = 4.85 MeV and B(C4) = $(4.38\pm0.88)\times10^4$ $e^2.fm^8$ [38]). Here, obviously the SRCs affect the calculated C4 form factors (the solid line) over both the first and second loops, where the attachment of SRCs leads to enhance

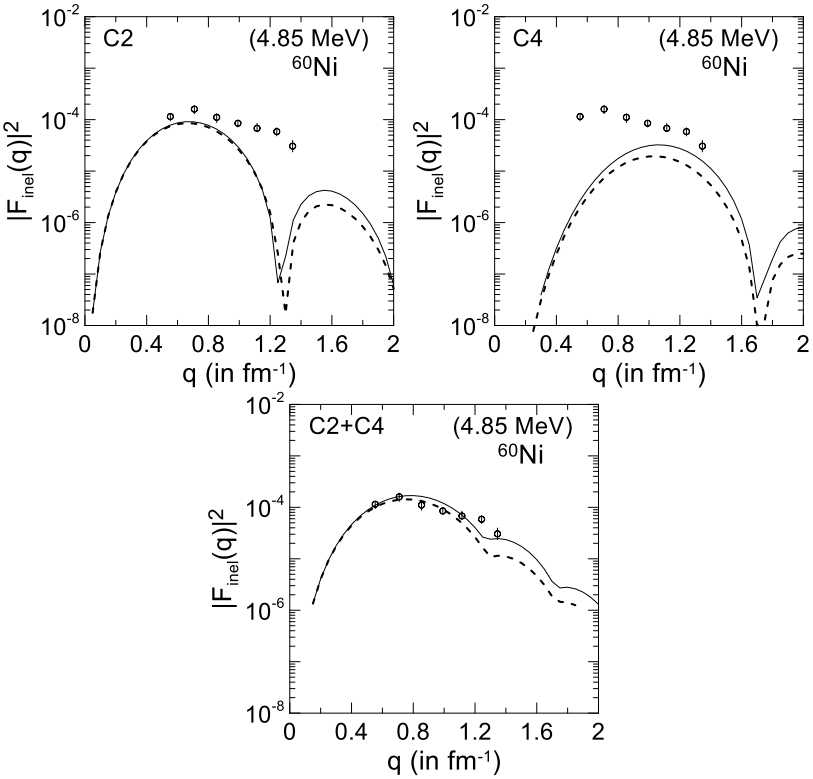

Figure 7: Square of form factors in ^{60}Ni for states [2^+ (4.85 MeV) displayed in the left panel, 4^+ (4.85 MeV) displayed in the middle panel, and the combined 2^+ (4.85 MeV) and 4^+ (4.85 MeV) displayed in the right panel]. The dashed and solid lines embody the estimated results produced without and with the attachment of SRCs, in that order. The measured results (open circles) are taken from [38].

the outcomes of the solid line and makes them nearer to the data particularly at the section of $q > 1$ fm^{-1}. The middle panel also reveals that the calculated outcomes of the solid line undervalue noticeably the data at the region of $0.5 \le q \le 1$ fm^{-1}. Hence, the solid line is not adequate to elucidate the data at all q-values under study. In the right panel, the measured data and those of combined C2 and C4 outcomes is displayed. It is clear that the dashed line

of the combined C2 and C4 outcomes is in tremendous accordance at $0.5 \le q \le 1.05$ fm^{-1} but beyond this section of q (i.e, at $q > 1.05$ fm^{-1}) the accordance is not good, where the data are clearly underrated by the dashed line. But, the solid line of the combined C2 and C4 results is in fine consistency with the measured data throughout all regions of momentum transfer under investigation

In Fig. 8, the computations are repeated as in Fig. 7 but this time for the state E_x = 5.05 MeV. Here, the experimental form factors of E_x = 5.05 MeV are decomposed to C4 and C6 results using the same technique of computations that we have used in Fig. 7. In the left (middle) panel, the C4 (C6) form factors of the state 4^+ (6^+) with B(C4) = $(1.22 \pm 0.24) \times 10^5$ e^2.fm^8 (B(C6) = $(1.54 \pm 0.46) \times 10^8$ e^2.fm^{12}) are presented and compared with those of experimental data [38]. It is conspicuous that the C4 and C6 results computed without and with enclosure of SRCs are in disagreement with the data of open circles, where the data are evidently undervalued by both the dashed and solid lines. However, the computed C4 results (left panel) are closer to the data than those of C6 (middle panel). Also, the solid lines in these panels are generally nearer to the data than those of the dashed line, where allowing for the SRCs into computations leads to boost the C4 and C6 results and makes them nearer to the data than those of without SRCs (the dashed line). Inspection of the left (middle) panel provides the indication that the C4 (C6) form factors

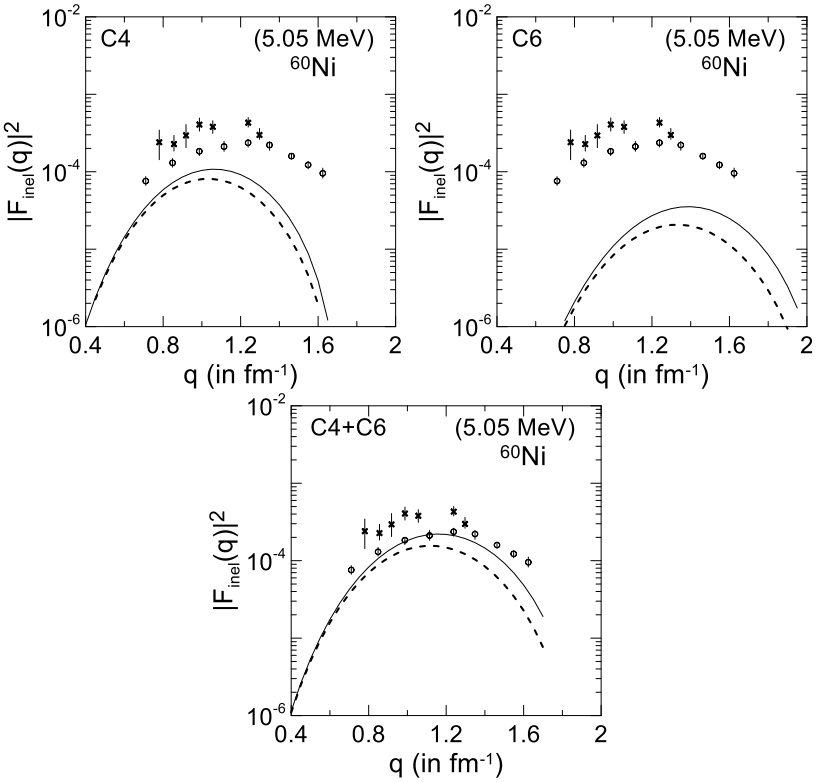

Figure 8: Square of form factors in ^{60}Ni for states [4^+ (5.05 MeV) displayed in the left panel, 6^+ (5.05 MeV) displayed in the middle panel, and the combined 4^+ (5.05 MeV) and 6^+ (5.05 MeV) displayed in the right panel]. The dashed and solid lines embody the estimated results produced without and with the attachment of SRCs, in that order. The measured results (open circles) are taken from [38].

alone are insufficient to explicate the data over all q-values under study. The judgment between the data (open circles) and those of combined C4 and C6 form factors is exhibited in

the right panel. Here, the dashed and solid lines are the combined C4 and C6 results computed without and with the effect of SRCs, in that order. Actually, combining together the computed C4 and C6 results (right panel) leads to a sturdy adjustment to the form factors of the state E_x = 5.05 MeV. Although, the strong modification occurred in the computations of the dashed and solid lines due to the combination of C4 and C6 results, the dashed line still did not accord with the data throughout all *q*-values considered in this investigation, where these data are underestimated by this line. However, the computed results of the solid line presented in the right panel demonstrate a well accord with the data over all *q*- values pondered in this study.

In Fig. 9, the calculations are done exactly as in Fig. 7 but now for the state E_x = 6.85 MeV. Here, the observed form factors of the state E_x = 6.85 MeV are decomposed to C2 and C5 results employing the similar procedure of calculations as that we have employed in Fig. 7. The left (middle) panel of this figure shows the C2 (C5) findings for the state 2^+ (5^-) of E_x = 6.85 MeV and B(C2) = $(3.88 \pm 0.58) \times 10$ $e^2.fm^4$ (B(C5) = $(3.53 \pm 0.88) \times 10^6$ $e^2.fm^{10}$) [38]. The dashed and solid lines represent the C2 (C5) findings estimated without and with the enhancement of the influence of SRCs whereas those of open circles represent the observed data [38]. The left panel reveals that the SRCs affect slightly (considerably) the C2 findings across the first (second) loop, where a small (substantial) deviation is seen between the dashed and solid lines. Moreover, the data at $0.4 \le q \le 0.9$ ($q > 0.9$) fm^{-1} are in fair (poor) agreement with C2 findings of both the dashed and solid lines, where these findings underestimate manifestly the data, particularly at $q > 0.9$ fm^{-1}. Thus, the C2 findings alone are inadequate for describing the observed data at all areas of considered *q*. The middle panel shows that the C5 findings of the dashed line are unable

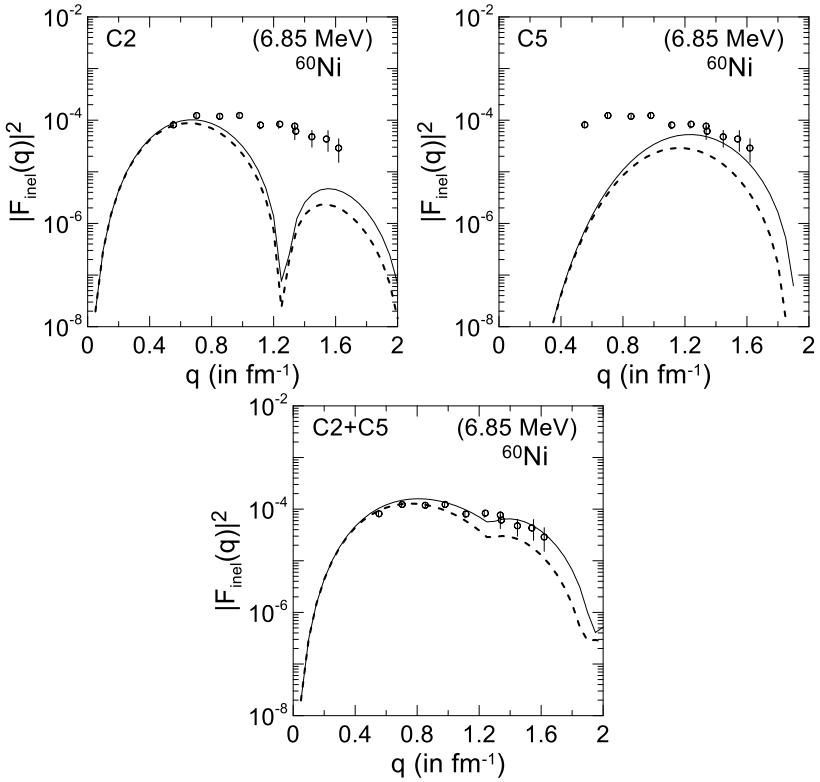

Figure 9: Square of form factors in ^{60}Ni for states [2^+ (6.85 MeV) displayed in the left panel, 5^- (6.85 MeV) displayed in the middle panel, and the combined 2^+ (6.85 MeV) and 5^- (6.85 MeV) displayed in the right panel]. The dashed and solid lines embody the estimated results

produced without and with the attachment of SRCs, in that order. The measured results (open circles) are taken from [38].

in clarifying the observed data at all q-values considered in this study, where these data are underrated by this line. Furthermore, the C5 findings of the solid line are unsuccessful (successful) in explaining the data at $0.45 \le q \le 1.1$ ($q > 1.1$) fm^{-1}. As a result, the C5 findings alone (the solid line) are insufficient for interpreting the data at all ranges of q-values under investigation. The right panel demonstrates the judgment amidst the combined C4 and C5 findings and those of the observed data. It is apparent from the right panel that the dashed line agrees well (deviates clearly) the data at the region $0.5 \le q \le 1.1$ ($q > 1.1$) fm^{-1}. However, the solid line of the combined C2 and C5 findings displayed in the right panel shows a well consistency with the observed data through all regions of q-values under examination. Inspection of Fig. 9 provides the conclusion that the anticipated form factors at momentum transfer region $q \le 1.1$ ($q > 1.1$) fm^{-1} are entirely from the C2 (C5) contribution.

4. Conclusions

The effect of short-range correlations on density, elastic and inelastic Coulomb form factors of the ^{60}Ni atomic nucleus has been scrutinized. The present computations are subject to the parameters b and β. These parameters are autonomously produced for each distinct nucleus by matching between the predicted and experimental elastic form factors, since a single value for each of b and β has been used in the present computations, where the present computations have been evidently controlled by the effect of short-range correlations. This effect is found to be indispensable for attainment a notable revision to the predicted findings which eventually lead to explicate the data surprisingly throughout the studied region of q.

Acknowledgment

We desire to give our appreciations to Prof. B. A. Brown of the National Superconducting Cyclotron Laboratory, Michigan State University, for providing the OXBASH-code.

References

[1] R.Weiss, R.Cruz-Torres, N.Barnea, E.Piasetzky, O.Hen, "The nuclear contacts and short range correlations in nuclei," *Physics Letters B*, vol. 780, pp. 211–215, 2018.

[2] O. Hen, B. A. Li, W.-J. Guo, L.B. Weinstein, E. Piasetzky, "Symmetry energy of nucleonic matter with tensor correlations," *Physical review C*, vol. 91, no. 2, pp. 25803-25815, 2015.

[3] B.-J. Cai, B. A. Li, "Symmetry energy of cold nucleonic matter within a relativistic mean field model encapsulating effects of high-momentum nucleons induced by short-range correlations," *Physical Review C*, vol. 93, no. 1, pp. 14619-14633, 2016.

[4] L.B. Weinstein, E. Piasetzky, D.W. Higinbotham, J. Gomez, O. Hen, R. Shneor, "Short range correlations and the EMC effect," *Physical Review Letters*, vol. 106, no. 5, pp. 52301-52306, 2011.

[5] O. Hen, A. Accardi, W. Melnitchouk, E. Piasetzky, "Constraints on the large-x d/u ratio from electron-nucleus scattering at x> 1, " *Physical Review D*, vol. 84, no. 11, pp. 117501-117517, 2011.

[6] O. Hen, D.W. Higinbotham, G.A. Miller, E. Piasetzky, L.B. Weinstein, "The EMC effect and high momentum nucleons in nuclei," *Int. J. Mod. Phys. E*, vol. 22, no. 7, pp. 1330017-1330029, 2013.

[7] O. Hen, G.A. Miller, E. Piasetzky, L.B. Weinstein, "Nucleon-nucleon correlations, short-lived excitations, and the quarks within," *Rev. Mod. Phys.*, vol. 89, no. 4, pp. 45002-45015, 2017.

[8] O. Hen, E. Piasetzky, L.B. Weinstein, "New data strengthen the connection between short rangecorrelations and the EMC effect," *Phys. Rev. C*, vol. 85, no. 4, pp. 47301-47319, 2012.

[9] H. Gallagher, G. Garvey, G.P. Zeller, "Neutrino-nucleus interactions,"*Ann. Rev. Nucl. Part. Sci.*, vol. 61, pp. 355-378, 2011.

[10] L. Fields, J. Chvojka, L. Aliaga, O. Altinok, B. Baldin, A. Baumbaugh, A. Bodek, et al., "Measurement of muon antineutrino quasielastic scattering on a hydrocarbon target at $E_\nu \sim$ 3.5 GeV," *Phys.Rev. lett.*, vol. 111, no. 2, pp. 22501-22506, 2013.

[11] G.A. Fiorentini, D.W. Schmitz, P.A. Rodrigues, L. Aliaga, O. Altinok, B. Baldin, A. Baumbaugh, et al., "Measurement of muon neutrino quasielastic scattering on a hydrocarbon target at E $\nu\sim$ 3.5 GeV," *Phys.Rev. lett.*, vol. 111, no. 2, pp. 22502-22511, 2013.

[12] R. Acciarri, C. Adams, J. Asaadi, B. Baller, T.Bolton, C. Bromberg, F. Cavanna, et al., "The etection of back-to-back proton pairs in charged-current neutrino interactions with the ArgoNeuT detector in the NuMI low energy beam line," *Phys. Rev. D*, vol. 90, pp. 12008-12021, 2014.

[13] L.B. Weinstein, O. Hen, E. Piasetzky, "Hammer events, neutrino energies and nucleon-nucleon correlations," *Phy. Rev. C*, vol. 94, no. 4, pp. 45501-45517, 2016.

[14] Altaf A. Al-Rahmani, Sanna N. Fadhil, Adel K. Hamoudi, "Indications for the substantial predominance of short-range effects on inelastic coulomb form factors for various states in the ^{26}Mg nucleus," *Iraqi Journal of Science*, vol. 65, no. 3, PP. 1357-1376, 2024.

[15] R.B. Wiringa, R. Schiavilla, S.C. Pieper, J. Carlson, "Nucleon and nucleon-pair momentum distributions in A$\leq$ 12 nuclei," *Phys. Rev. C*, vol. 89, no. 2, pp. 24305-24321, 2014.

[16] J. Carlson, S. Gandolfi, F. Pederiva, S.C. Pieper, R. Schiavilla, K.E. Schmidt, R.B. Wiringa, "Quantum Monte Carlo methods for nuclear physics" *Reviews of Modern Physics*, vol. 87, no. 3, pp. 1067-1079, 2015.

[17] G. Hagen, A. Ekström,, C. Forssén, G. R. Jansen, W. Nazarewicz, et al., "Neutron and weak-charge distributions of the 48Ca nucleus," *Nat. Phys.*, vol. 12, no. 2, pp. 186–190, 2016.

[18] D. Lonardoni, A. Lovato, S.C. Pieper, R.B. Wiringa, "Variational calculation of the ground state of closed-shell nuclei up to A= 40," *Phys. Rev. C*, vol. 96, no.2, pp. 24326-24338, 2017.

[19] J. Ryckebusch, M. Vanhalst, W. Cosyn, "Stylized features of single-nucleon momentum distributions ," *Journal of Physics G*, *Nucl. Part. Phys.*, vol. 42, no. 5, pp. 55104-55123, 2015.

[20] M. Vanhalst, J. Ryckebusch, W. Cosyn, "Quantifying short-range correlations in nuclei," *Phys. Rev. C*, vol. 86, no. 4, pp. 44619-44635, 2012.

[21] C. Colle, O. Hen, W. Cosyn, I. Korover, E. Piasetzky, J. Ryckebusch, L.B. Weinstein, "Extracting the mass dependence and quantum numbers of short-range correlated pairs from A (e, e′ p) and A (e, e′ p p) scattering," *Phys. Rev. C*, vol. 92, no. 2, pp. 24604-24618, 2015.

[22] S.E. Massen, H.P. Nassena and C.P. Panos, "A formula for the charge form factor of closed-shell
nuclei and its application to ^{16}O," *J. Phys. G*, vol. 14, pp. 753-764, 1988.

[23] S.E. Massen and C.P. Panos, "An approximate treatment of the correlated charge form factor of light nuclei," *J. Phys. G: Nucl. Phys*, vol. 15, pp. 311-319, 1989.

[24] S.E. Massen," Correlated charge form factor and densities of the s-d shell nuclei," *J. Phys. G: Nucl. Phys.* vol. 16, pp. 1713-1725, 1990.

[25] J.W. Clark and M.L. Ristig, "Cluster-Expansion Procedures for the Correlated Charge Form Factor," *Nuovo Cimento A*, vol. 70, pp. 313-322, 1970.

[26] M.L. Ristig, W.J. Ter Low, J.W. Clark," Tensor Correlations in Nuclear Matter," *Phys. Rev. C*, vol. 3
, pp. 1504-1513, 1971.

[27] W. Clark, "Variational theory of nuclear matter," *Prog. Part. Nucl. Phys.*, vol. 2, pp. 89-99, 1979.

[28] S.E. Massen and Ch. C. Moustakidis, "Systematic study of the effect of short range correlations on
the form factors and densities of s-p and s-d shell nuclei," *Phys. Rev. C*, vol. 60, pp. 24005-24017,
1999.

[29] R. Jastrow, "Many-Body Problem with Strong Forces," *Phys. Rev.*, vol. 98, pp. 1479-1484, 1955.

[30] Adel K Hamoudi and Mahmoud A. Abbas," Electron scattering from some fp-shell nuclei with inclusion the effect of short-range correlation," *Iraqi Journal of Science*, vol. 61, no. 10, pp. 2540-

2550, 2020.

[31] Israa Khalil. Abdalsada, Altaf A. Al-Rahmani," Inelastic Form Factors for the ^{90}Zr Nucleus with Short-Range Considerations Effect," *Iraqi Journal of Science*, vol. 65, no. 12, pp. 7005-7020, 2024.

[32] B.A. Brown, B.H. Wildenthal, C.F. Williamson, F.N. Rad, S. Kowalski, Hall Crannell, J.T. Brien,
"Shell-model analysis of high-resolution data for elastic and inelastic electron scattering on ^{19}F," *Physical Review C*, vol. 32, pp. 1127–1156, 1985.

[33] P.J. Brussard and P.W.M. Glaudemans, *Shell-Model Applications in Nuclear Spectroscopy, North*
Holland, Amsterdam, 1977, p. 14.

[34] T.W. Donnelly and I. Sick Rev., "Elastic magnetic electron scattering from nuclei," *Rev. Mod. Phys.*, vol. 56, pp. 461–566, 1984.

[35] B. A. Brown, R. Radhi and B.H. Wildenthal, "Electric quadrupole and hexadecupole nuclear excitations from the perspectives of electron scattering and modern shell-model theory," *Phys. Rep.*, vol. 101, pp. 313–358, 1983.

[36] L. J. Tassie, "A Model of Nuclear Shape Oscillations for E2 Transitions and Electron Excitation," *Austr. J. Phys*., vol. 9, pp. 407-413, 1956.

[37] H. De Vries, C.W. De Jager, and C. De Vries, "Nuclear charge density distribution parameters from elastic electron scattering," *Atomic Data and Nuclear Data Tables*, vol. 36, pp. 495-536, 1987.

[38] Y. Torizuka, Y.Kojima, M. Oyamada, K. Nakahara, K. Sugiyama, T.Terasawa, K. Itoh, A. Yamaguchi, and M. Kimura. "Study of Nuclear States in ^{60}Ni by Inelastic Electron Scattering,"
Phys.Rev., vol. 185, no. 4, pp. 1499-1507, 1969.